Multiscale tomography of buried magnetic structures: its use in the localization and characterization of archaeological structures

Ginette Saracco, Frédérique Moreau, Pierre-Etienne Mathé, Daniel Hermitte, Jean-Marie Michel

Geophys. J. Int. (2007) **171,** 87–103 doi: 10.1111/j.1365-246X.2007.03501.x

Multiscale tomography of buried magnetic structures: its use in the localization and characterization of archaeological structures

Ginette Saracco,[1] Frédérique Moreau,[2] Pierre-Etienne Mathé,[1] Daniel Hermitte[1] and Jean-Marie Michel[3]

[1] *CNRS-UMR* 6635, *CEREGE, UPCAM, Géophysique & Planétologie, Europole de l'Arbois,* BP 80, 13545 *Aix en Provence, France. E-mail: ginet@cerege.fr*
[2] *CNRS-UMR* 6118, *Géosciences-Rennes, Campus de Beaulieu, Bat* 15, 35042 *Rennes, France*
[3] *INRAP, Service Archéologique du Var,* 83000 *Toulon, France*

Accepted 2007 May 16. Received 2007 May 11; in original form 2006 May 12

SUMMARY

We have previously developed a method for characterizing and localizing 'homogeneous' buried sources, from the measure of potential anomalies at a fixed height above ground (magnetic, electric and gravity). This method is based on potential theory and uses the properties of the Poisson kernel (real by definition) and the continuous wavelet theory. Here, we relax the assumption on sources and introduce a method that we call the 'multiscale tomography'. Our approach is based on the harmonic extension of the observed magnetic field to produce a complex source by use of a complex Poisson kernel solution of the Laplace equation for complex potential field. A phase and modulus are defined. We show that the phase provides additional information on the total magnetic inclination and the structure of sources, while the modulus allows us to characterize its spatial location, depth and 'effective degree'. This method is compared to the 'complex dipolar tomography', extension of the Patella method that we previously developed. We applied both methods and a classical electrical resistivity tomography to detect and localize buried archaeological structures like antique ovens from magnetic measurements on the Fox-Amphoux site (France). The estimates are then compared with the results of excavations.

Key words: complex dipolar occurrence tomography, complex wavelet transform, electrical resistivity, inverse problem in potential field, magnetic anomalies, multiscale tomography.

1 INTRODUCTION

Recent advances in geophysical instrumentations and new developments in numerical processing concerning inverse problems in potential theory (Blakely 1995) have made possible a 2-D or 3-D tomography of the earth subsurface. For example, hydric flow circulation can be detected from electrical self-potential tomography (Zhdanov & Keller 1994; Ishido & Pritchett 1999; Lapenna *et al.* 2000; Sailhac & Marquis 2001; Saracco *et al.* 2004), while buried archeological structures, specific cavities or density of sources can be localized from magnetic or gravity potential anomalies (Noel & Xu 1991; Mauriello *et al.* 1998; Durrheim & Cooper 1998; Martelet *et al.* 2001; Jeng *et al.* 2003). These developments based on potential theory are coupled to specific methods such as Euler method (Thompson 1982; Reid *et al.* 1990; Ravat *et al.* 1996), generalized Hilbert transform (Nabighian 1984), gradient method (Marson & Klingele 1993), real (Moreau *et al.* 1997, 1999; Hornby *et al.* 1999) or complex wavelet transform (Saracco *et al.* 2004). Another method is to consider the detection of buried sources as the search of inverse filters (Tsokas & Papazachos 1992), or as the result of correlations between a supposed synthetic source (monopolar or dipolar) and the measured potential anomalies (Mauriello & Patella 1999; Mauriello *et al.* 1998; Patella 1997) .

This last method, called monopolar or dipolar charge occurrence probability, requires the specification of the multipolar order of the source. In the wavelet analysis method of potential fields (Moreau *et al.* 1997, 1999) no *a priori* information of the degree of sources is required. The wavelet method allows the estimation of the degree of sources, but in both cases, the potential anomalies are assumed to be generated from isolated homogeneous sources.

The fact that many magnetic sources can be considered in first approximation, as magnetic dipoles, makes it interesting to define an extension of the Patella method: the complex dipolar occurrence tomography (CDOT) (Saracco *et al.* 2004). This method is based on phase and modulus, as the complex continuous wavelet transform (CCWT). The CDOT method allows us to obtain rapid information about the position and inclination of buried dipolar archaeological objects. Multiscale tomography allows us to estimate the inclination and depth of arbitrary geometrical structures, if there exists a

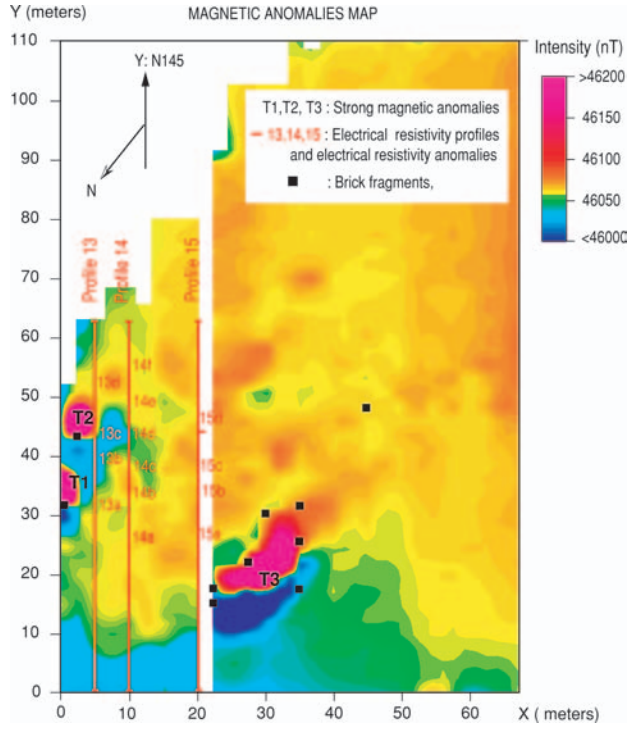

Figure 1. 2-D map of magnetic anomalies data.

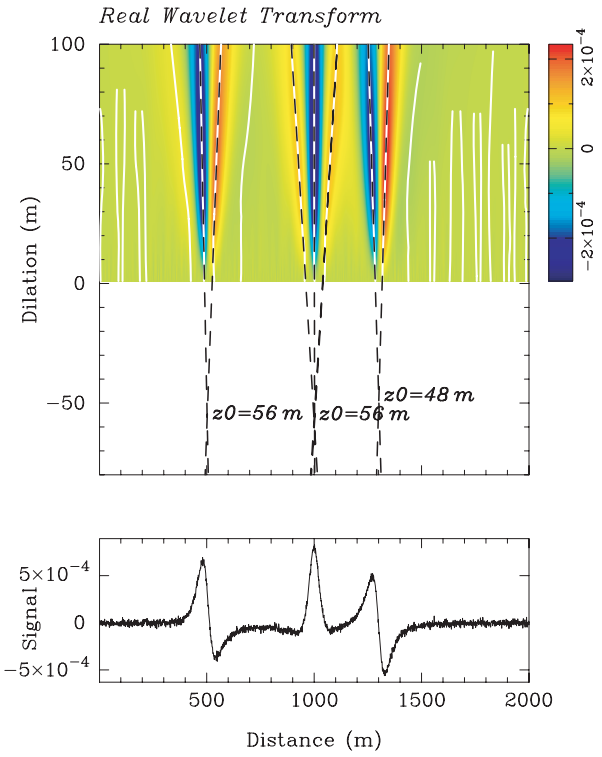

Figure 2. Real multiscale tomography (RMST). Bottom: Noisy synthetic magnetic intensity generated by three magnetic dipoles of different inclination (30°, 90° and 0°) located in the subsurface earth at depth $z = 50$ m and lateral distances 500, 1000 and 1250 m, respectively. Top: Amplitude of the RMST. The intersection of the lines of extrema (extrema of energy of the real wavelet transform) allows to localize each source depth (or dilation z). The depths obtained are in good agreement to the true depths (56, 56 and 48 m).

convergence of the lines of maxima in the modulus of the complex potential field.

The full recovery of magnetic structures from potential anomalies measured at the surface is an ill-conditioned inverse problem (Tarantola 1987; Sabatier 1987; Telford *et al.* 1990; Parker 1994). Any practical method has to be limited to the estimation of a few parameters.

The purpose of this paper is to introduce a new method of tomography for potential field, that we call multiscale tomography, where sources are not assumed to be homogeneous. The method is quite general; here it is applied to magnetic fields. The method allows us to obtain estimates of spatial location, depth, inclination and 'effective' degree (see Section 3) of buried structures from above-ground measurements of the magnetic field at fixed height. Here, it is applied to localize and characterize archaeological structures. The estimates are then compared with the results of excavations and with estimates given by other methods. The interest of this method for archaeologists is (i) to have a non-destructive test of an archaeological site and (ii) to suggest a strategy of excavation.

Before giving a rough description of the method, we recall a few basic facts.

A stationary magnetic field is the gradient of a scalar magnetic potential. This potential satisfies the Poisson equation, which becomes the Laplace equation in regions without sources (typically in the half-space $z > 0$ in which we take measures).

If we know the potential in any horizontal plane with $z = z_0$ and $z_0 > 0$, we can calculate the potential in the whole half-space $z > 0$, without making any assumption about the source. This is done by taking the convolution product of the known potential measured at a fixed height z_0 by the dilated Poisson kernel, where the dilation operator acts on the depth. The calculation of the potential field in the whole half-space $z > 0$ is analogous to the continuous wavelet transform of the potential measured at the fixed height z_0, where the translation operator acts on the horizontal space (x, y), while the dilation parameter represents, here $|z - z_0|$, the depth or height. The continuous wavelet transform combined with potential theory can be used.

The multiscale tomography method developed here, is based on the dilation property of the derivatives of a complex Poisson kernel (solution of the Laplace equation for complex potential fields) (Saracco *et al.* 2004) and on properties of the wavelet theory which analyses local singularities (Grossmann 1986; Grossmann *et al.* 1987; Mallat & Hwang 1992). We extract information on the phase or ridge of the wavelet transform (Grossmann *et al.* 1987; Saracco *et al.* 1990b, 1991; Delprat *et al.* 1991). The presence of a cone line structure of the potential field anomalies is a necessary condition to estimate the depth and other parameters of sources. If the sources are homogeneous tempered distributions, the 'effective degree ' is then the homogeneous degree defined in Moreau *et al.* (1997).

After a brief recall of the geomagnetic field equations we present (Section 2), the map of magnetic anomalies obtained from the magnetic survey at Fox-Amphoux site (Var, south of France) conducted on cultivated fields. A classical and rough inversion method to localize the depth of buried structures is given. We define, in Section 3, the multiscale tomography. The complex dipolar occurrence tomography (CDOT), an extension of the Patella method, in terms of modulus and phase is defined in Section 4. In order to validate our procedure, we have applied both methods to simulated noisy magnetic anomalies generated by the sum of buried dipolar sources of different inclinations and depths, and by the sum of different buried multipolar sources. The methods are applied to localize and characterize archaeological structures like antique ovens. Section 5 shows

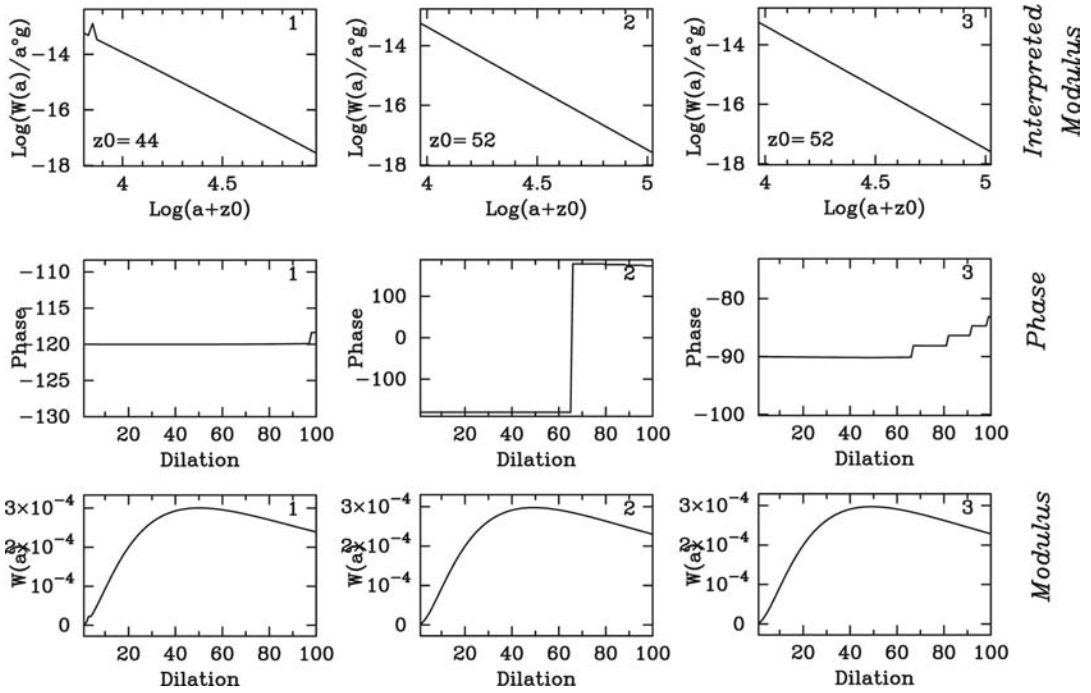

Figure 3. Characterization of the magnetic sources with inclination 30° (=1), 90° (=2) and 0^0 (=3), from the phase and lines of extrema. Top: Slope $\beta = -4$ allowing to extract the degree $\alpha = \beta - 1$ of the source and depth (z). Middle: Inclination $\theta = -(90^0 + Phase)$. Bottom: Amplitude variation along the ridge versus dilation.

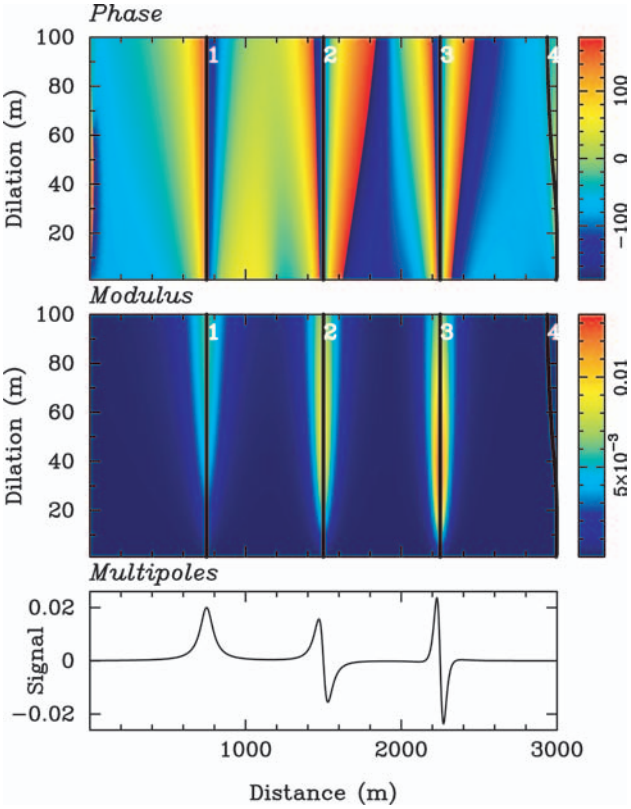

Figure 4. Complex multiscale tomography. Bottom: Synthetic magnetic intensity generated from a monopole, a dipole and a quadrupole source at lateral distances 750, 1500 and 2250 m, respectively, and depth $z = 50$ m. Middle: Modulus. Top: Phase. The vertical black lines indicate the value of the inclination of each source. The localization and characterization of each source is correctly obtained.

the results obtained by real and complex multiscale tomography and by the complex dipolar tomography technique on magnetic profiles. Conjointly, an electrical resistivity prospecting and a rock magnetic study including measurements of susceptibility and magnetizations (induced and remanent) were carried out. The results are discussed in Section 6, and compared with the excavation results of Roman ovens. Perspectives and conclusions are found in Section 7.

2 GEOMAGNETIC POTENTIAL FIELD: FORMULATION AND EXPERIMENTATION

Let **B** be the magnetic induction of declination D (angle between the magnetic and the geographic north), and inclination I [angle between **B** and the horizontal plane (x, y)]. In absence of external sources (external current density due to solar wind, solar cycles, etc., is negligible) and in the quasi-static limit, the equation for magnetic induction $\nabla \wedge \mathbf{B} = \mathbf{0}$ holds. It follows that $\mathbf{B} = -\nabla\phi$ where ϕ is the scalar magnetic potential. For an arbitrary observation point, B is written as the sum of the ambient magnetic field **H** modulated by diurnal variations and the total magnetization **M** ($\mathbf{M} = \mathbf{M}_i + \mathbf{M}_r$) modulated by ambient noise and topographic effects. The induced magnetization $\mathbf{M}_i$ is parallel and proportional to H while the remanent magnetization $\mathbf{M}_r$ depends on the ferromagnetic composition of the material and **H** at the original time. Let ϵ be the set of fluctuations:

$$\mathbf{B} = \mu\mathbf{H} + \epsilon = \mu_0(\mathbf{H} + \mathbf{M}) + \epsilon = \mu_0(1 + \mathbf{K})\mathbf{H} + \epsilon,$$

μ and K represent the permeability and the magnetic susceptibility of the ground. μ_0 represents the vacuum permeability, so that $\mathbf{B_0}$ in vacuum is equal to $\mu_0\mathbf{H}(nT)$. $\mu_0 = 4\pi\,10^{-7}\Omega\mathrm{sm}^{-1}$. $\mathbf{M}_r$ is, here, principally due to the natural thermoremanent magnetization acquired during the cooling of archaeological structures to a

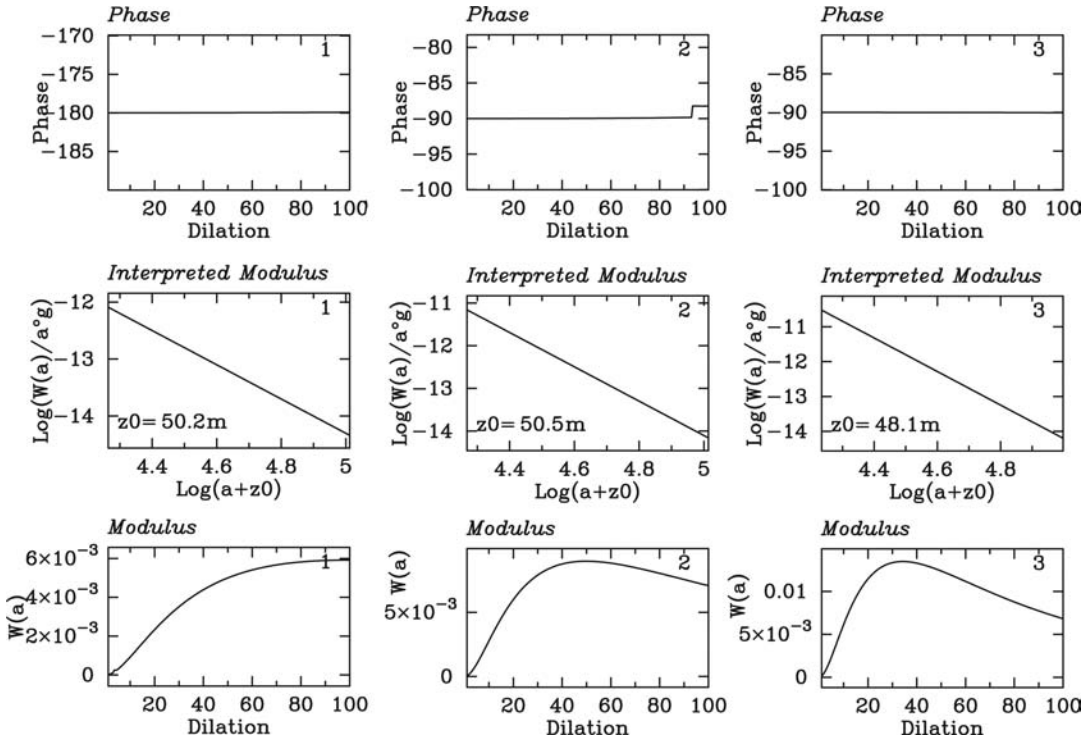

Figure 5. From top to bottom for each type of magnetic source (monopole = 1, dipole = 2 and quadrupole = 3). Top: Inclination $\theta = -(90^0 + Phase$. Middle: Slope β allowing to extract the degree $\alpha = \beta - 1$ of multipolar sources ($\beta = -3, -4.02$, and -4.85) with the depth ($z = 50.2$, 50.5 and 48.1 m). Bottom: Amplitude variation along the ridge versus dilation.

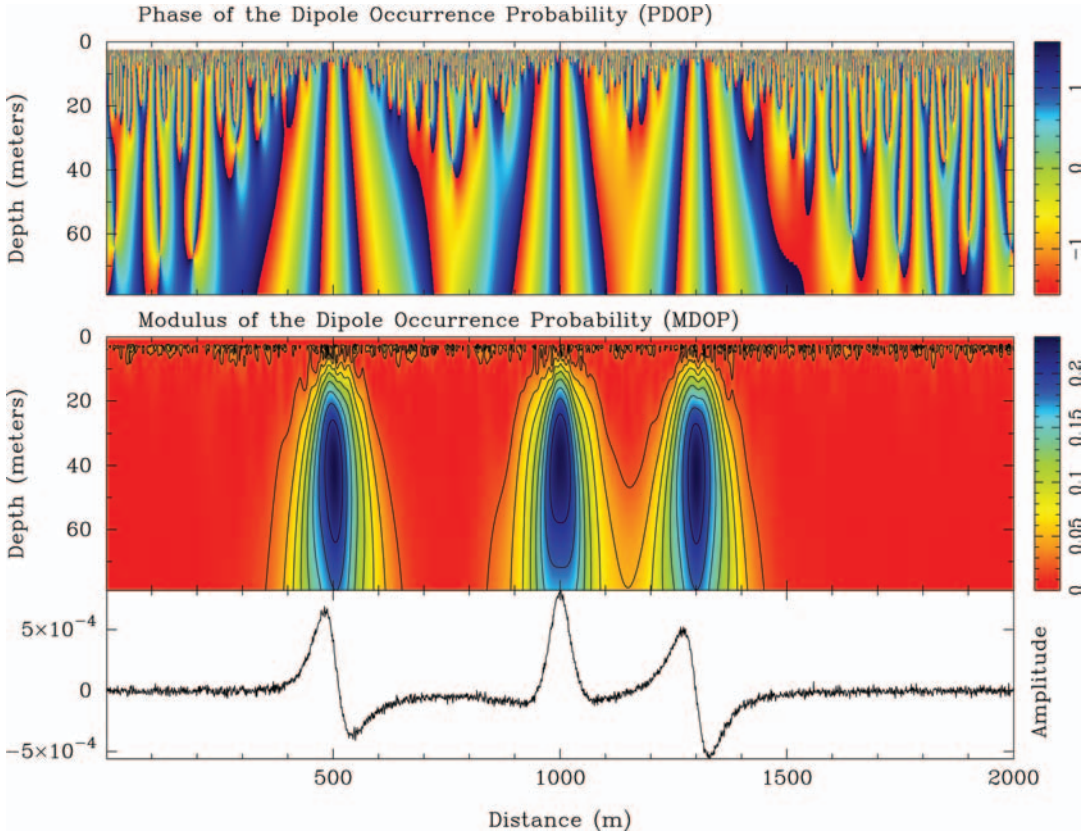

Figure 6. Complex dipolar occurrence tomography. Bottom: Same synthetic magnetic intensity as Fig. 2. Middle: Modulus (Dipolar occurrence tomography). Top: Phase. The vertical lines of phase located at lateral distances 500, 1000 and 1250 m, respectively, indicate the value of the inclination θ of each dipole ($\theta = -Phase, \pi/6, \pi, 0$). The depth of sources obtained in presence of noise are, respectively, around 45, 38 and 40 m instead of 50 m but with a dipolar occurrence probability in the modulus of the CDOT, $p = 0.25$.

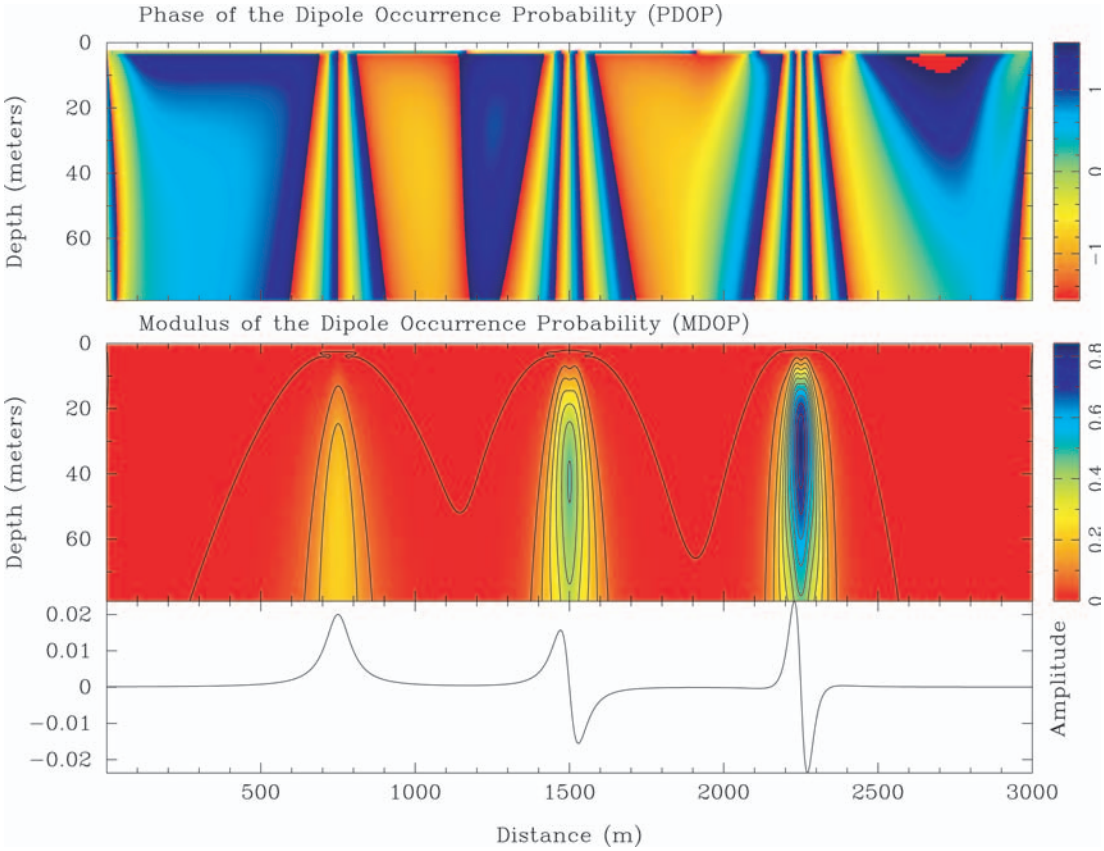

Figure 7. Complex dipolar occurrence tomography. Bottom: Same synthetic magnetic intensity as Fig. 4. The CDO tomography does not allow us to obtain a good depth estimate of multipolar sources. Middle: Modulus of the CDOT. It is impossible to localize and characterize the monopole source, its dipolar occurrence probability is around $p = 0.2$, and to obtain correct results for the others. Their depths are around 42 m (dipole) and between 25 m and 38 (quadrupole) with a CDOT value p of 0.6 and 0.8, respectively. Top: Phase of the CDOT. The vertical lines of phase located at lateral distances 750, 1500 and 2250 m, respectively, indicate the inclination value of each multipole. ($\theta = -Phase = \pi$, 0 and 0).

temperature below the Curie temperature. The present magnetic field given by the IGRF at site coordinates is 45 983 nT with a declination $D \simeq 0.14^\circ$ and an inclination $I \simeq 59^\circ$.

The magnetic data were obtained using a caesium vapor probe (G858 magnetometer from Geometrics) with a sensitivity of 0.01 nT. This kind of magnetometer allows a local measurement of the total magnetic field (induced and remanent). $\mathbf{M}_r$ is 20–50 times higher than $\mathbf{M}_i$, as indicated by Koenigsberger ratio $Q = M_r/M_i$, determined on a set of 10 discrete samples collected around T1, T2 and T3 (see Fig. 1). The temporal drift of the magnetic intensity during an experiment is recorded in order to take into account the diurnal variations of the magnetic field, and the local variation due to the magnetization of the lithospheric crust. At the scale of the site, the last fluctuations are negligible. We got an average variation of 4 nT hr^{-1}. The set of magnetic prospection covers an area of 70 × 110 m and was recorded in two parts (see map Fig. 1). Data acquisition was performed every 1 m along profiles oriented North 145° at a distance of 2.5 m from each other. The magnetic receiver was located at 0.8 m above the ground surface and the error due to moving position during data acquisition was less than 5 nT. Magnetic anomalies are mapped (Fig. 1) using a kriging extrapolation method and a linear correction for diurnal variations. Our analysis was performed on data without extrapolation.

Assuming that the volume of an oven is a cube of edge r', and the magnetization is induced in the present-day field, the magnetic anomaly **A** due to a dipolar source of susceptibility k, located in an homogeneous medium of susceptibility k_0, is: $\mathbf{A} = (\mathbf{k} - \mathbf{k}_0)\mathbf{F}\frac{r'^3}{r^3}$, where **F** is the intensity of the total magnetic field, r the distance between the magnetometer probe and the centre of the dipole.

Considering that $\mathbf{K} = (\mathbf{k} - \mathbf{k}_0) = 10^{-2}\ SI$, $\mathbf{F} \simeq 45\,983$ nT, and a fixed distance r' ($1 < r' < 1.5$ m), we can obtain a rough estimation of depths between the probe and the centre of the magnetic object for the three main anomalies T_1, T_2 *and* T_3 observed in Fig. 1. The mean depths corrected for the height of the probe are, respectively, 0.54, 0.82 and 1 m for the three anomalies.

This empirical method can be easily used to estimate in first approximation the depth of simple structures, but suffers from the fact that the non-uniqueness of the solution requires some '*a priori*' information on the size of the object. In order to reduce these limitations, it is necessary to formulate this problem in terms of a problem of potential theory with more general sources.

3 MULTISCALE TOMOGRAPHY OF MAGNETIC POTENTIAL SOURCES

3.1 Recall of real and complex continuous wavelet transform

First developed by A. Grossmann and J. Morlet in 1983, the continuous wavelet transform (CWT) is a well-known method which allows to decompose an arbitrary signal s in elementary

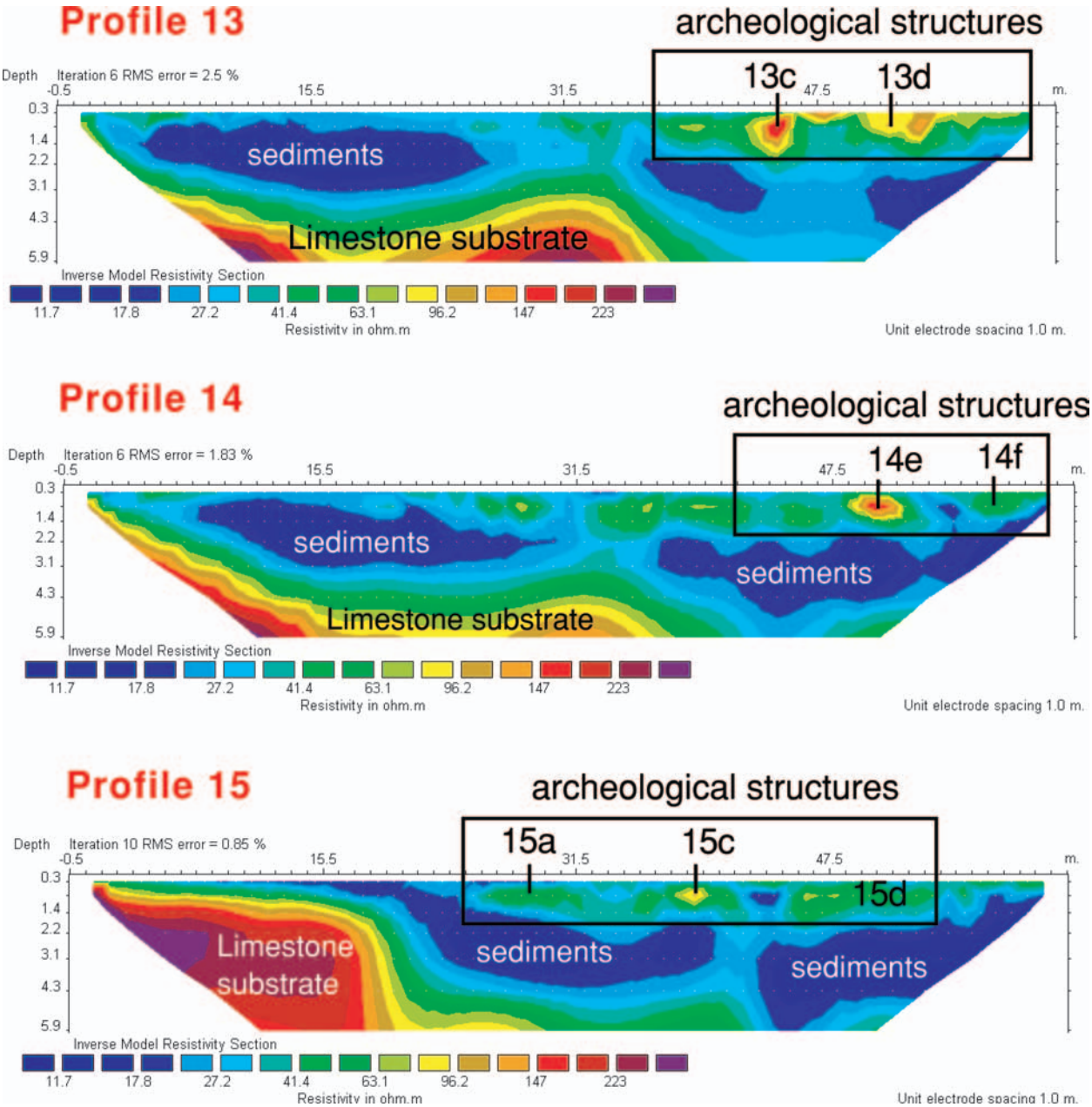

Figure 8. Electrical resistivity section. Profiles 13, 14 and 15 (see Fig. 1).

contributions called wavelets. These wavelets are obtained by dilation D^a and translation T^b of a 'mother or analysing wavelet' g, which is real or complex, and required to satisfy $\hat{g}(0) = 0$ (admissibility condition), where $\hat{g}$ is the Fourier transform of g.

The dilation and translation operators acting on a function f in $\mathcal{R}^n$ is defined as:

$$D^a f = a^{-n} f(\mathbf{r}/a) \text{ and } T^b f = f(\mathbf{r} - b).$$

The wavelet transform of an arbitrary signal s, in $\mathcal{R}^n$, is:

$$\begin{aligned} L_{(b,a)}s &= \langle T^b D^a g, s\rangle = \langle g(b,a)|s\rangle \\ &= (D^a g * s)(\mathbf{b}) \\ &= a^{-n} \int g\left(\frac{\mathbf{r}-b}{a}\right) s(\mathbf{r}) d\mathbf{r^n}, \end{aligned} \tag{1}$$

where $*$ represents the convolution product of the signal by the dilated family of wavelets g.

A characterization of the local regularity of the signal, or extraction of the degree of homogeneity of isolated singularities, can be obtained from the modulus of the CCWT along the lines of constant phase (Grossmann 1986; Grossmann *et al.* 1987), the restriction of the wavelet modulus along the phase ridge of the CCWT (Saracco 1989; Saracco *et al.* 1990a, 1991; Delprat *et al.* 1991; Guillemain 1994), or from the lines of extrema extracted from the RCWT when the analysing wavelet is real (Mallat & Hwang 1992; Moreau 1995; Alexandrescu *et al.* 1995; Moreau *et al.* 1997). Singularities are generally characterized by the local Lipschitz exponents. In the class of singularies, there is a homogeneous tempered distribution s in $\mathcal{R}^n$, of order α, satisfying for all test function ϕ, the homogeneous property:

$$s(\phi_\lambda) = s[\lambda^n \phi(\lambda.)] = \lambda^{\alpha n} s(\phi), \;\; \lambda > 0 \;\; \Rightarrow L_{(b,a)}s = \lambda^{\alpha n} L_{(b/a,1)}s \tag{2}$$

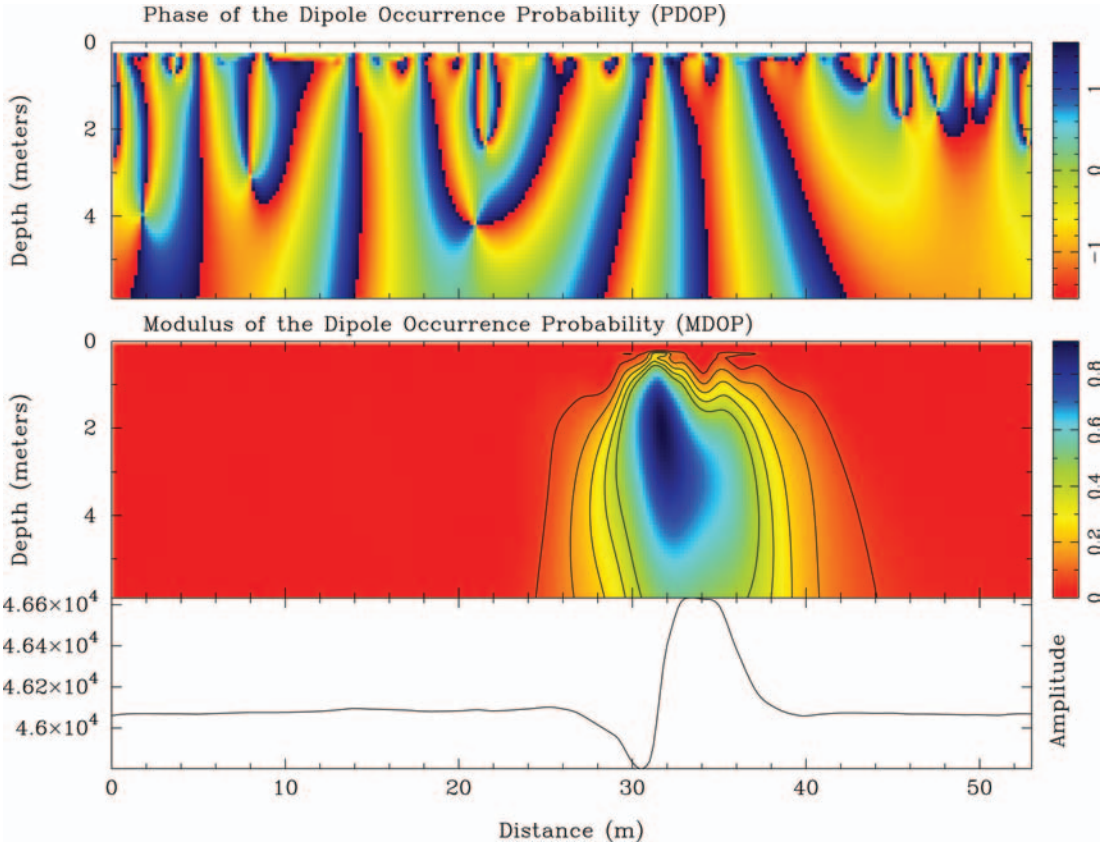

Figure 9. Magnetic complex dipolar occurrence tomography of anomaly T1 (profile $x = 0$ m, see Fig. 1). Top: Phase. Middle: Modulus. Bottom: Magnetic intensity.

In both cases the exponent, here the homogeneity degree, is estimated from the evolution across scales of the wavelet transform, in log–log representation and characterizes the local structure of s.

3.2 Potential theory and wavelet transform

The magnetic field measured at the altitude $z > 0$ (see Section 2), and generated by a buried source $\boldsymbol{\sigma}(\mathbf{x}, z)$, ($\mathbf{x} = (x, y)$), located in $z < 0$, satisfies:

$$\mathbf{B}(\mathbf{x}, z) = -\nabla A(\mathbf{x}, z), \tag{3}$$

with A denoting the scalar potential.

We have the system of equations:

$$\begin{aligned} &z > 0, \quad \Delta A(\mathbf{x}, z) = \mathbf{0}; \quad \mathbf{x} = (x, y); \\ &z = 0, \quad A(\mathbf{x}, 0) = A_0(\mathbf{x}); \\ &z < 0, \quad \Delta A(\mathbf{x}, z) = -\boldsymbol{\sigma}(\mathbf{x}, z). \end{aligned} \tag{4}$$

It follows:

$$A(\mathbf{x}, z) = (D^z P * A_0)(\mathbf{x}) = < T^x D^z g, A_0 > = L_{(\mathbf{x},z)} A_0 \tag{5}$$

P is defined in $\mathcal{R}^2$, $P(\mathbf{x}) = C_3(1 + |\mathbf{x}|^2)^{-5/2}$ (Courant & Hilbert 1990). The Fourier transform of P is $\hat{P}(\mathbf{u}) = exp^{-2\pi|\mathbf{u}|}$ where $\mathbf{u}$ is the dual variable of $\mathbf{x}$. A is called the harmonic extension of A_0 in the half-space $z > 0$.

The function P satisfies the crucial equation:

$$D^z P * D^{z'} P = D^{z+z'} P, \tag{6}$$

which can be easily verified in Fourier space. This property of the Poisson kernel is the starting point in this paper and in Moreau *et al.* (1997) on the use of wavelet theory in the study of potential fields.

Note that we work with measured values of the total magnetic field B, on profiles along the variable y, to obtain information in the plane (y, z) (see Fig. 1), that is, we work with the derivative of the magnetic scalar potential (∇A), and we assume $n = 1$, from now on.

If $A(y, z)$ is the solution of the Laplace equation in the half-plane $(y, z > 0)$, it is obtained from the convolution product of the dilated Poisson kernel and the known potential field at a fixed depth z_0. Let $A(y, z)$ be the solution of the Poisson equation in the half-plane $(y, z > 0)$. We can then write, using the dilation and translation operators, $A(y, z) = (D^z g * A_0)(y)$, that defines the real continuous wavelet transform (RCWT) of the measured magnetic field A_0 along the profile y. The depth z represents the dilation or scale parameter along the vertical axis, and y represents the translation parameter along the horizontal axis. P or the partial derivatives of P ($\partial_y^\gamma \partial_z^\delta P$), play the role of the analysing wavelet g which is real by definition. The half-plane $(y, z > 0)$ is the position-scale half-plane of the RCWT.

In order to localize and characterize buried sources σ in the half-plane $(z < 0)$, we use the property of harmonic extension of the solution $A(y, z)$ with the property of the Possion kernel defined in (6). It is not necessary to use all the information of the half-plane $z > 0$, that is, all wavelet coefficients $L_{(\mathbf{y},z)}$. Only the restriction of the wavelet coefficients along the lines of extrema of the modulus presenting a cone line structure is necessary. If the lines of extrema do not present a cone-line structure, no solution exists for the localization. The convergence of the lines of extrema

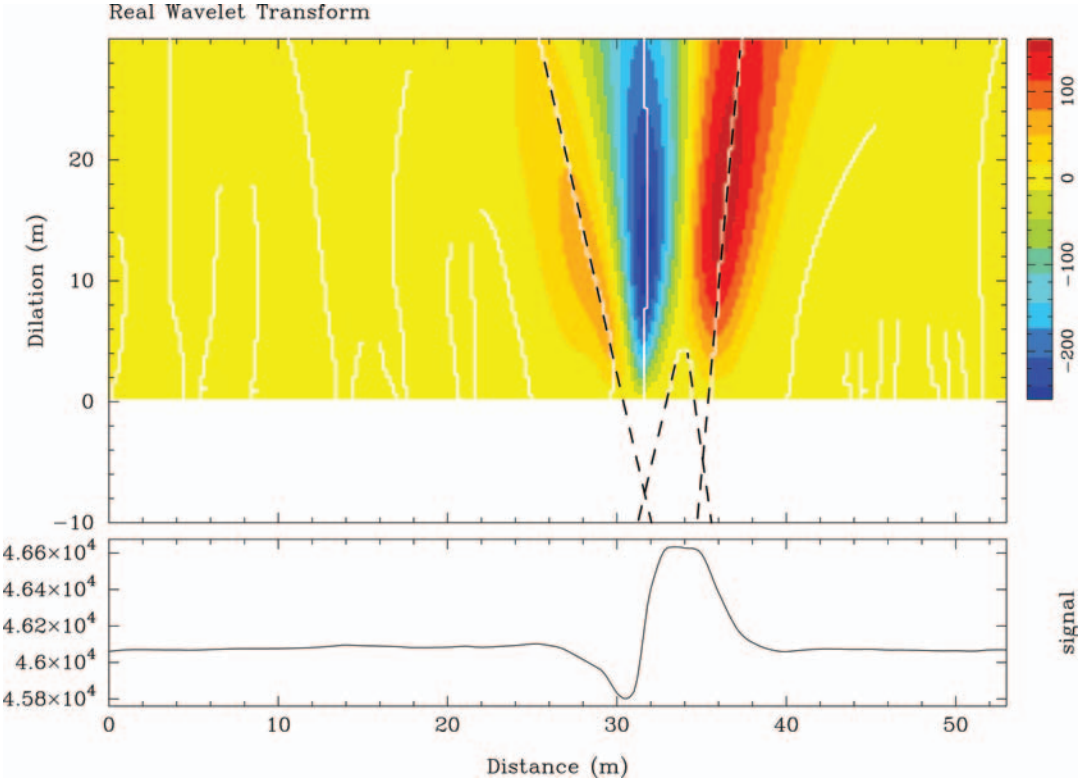

Figure 10. Real multiscale tomography of anomaly T1, (profile $x = 0$ m). Dashed lines represent the lines of extrema. The dilation -10 represents, here, a depth of 2 m with a sample rate of 0.2.

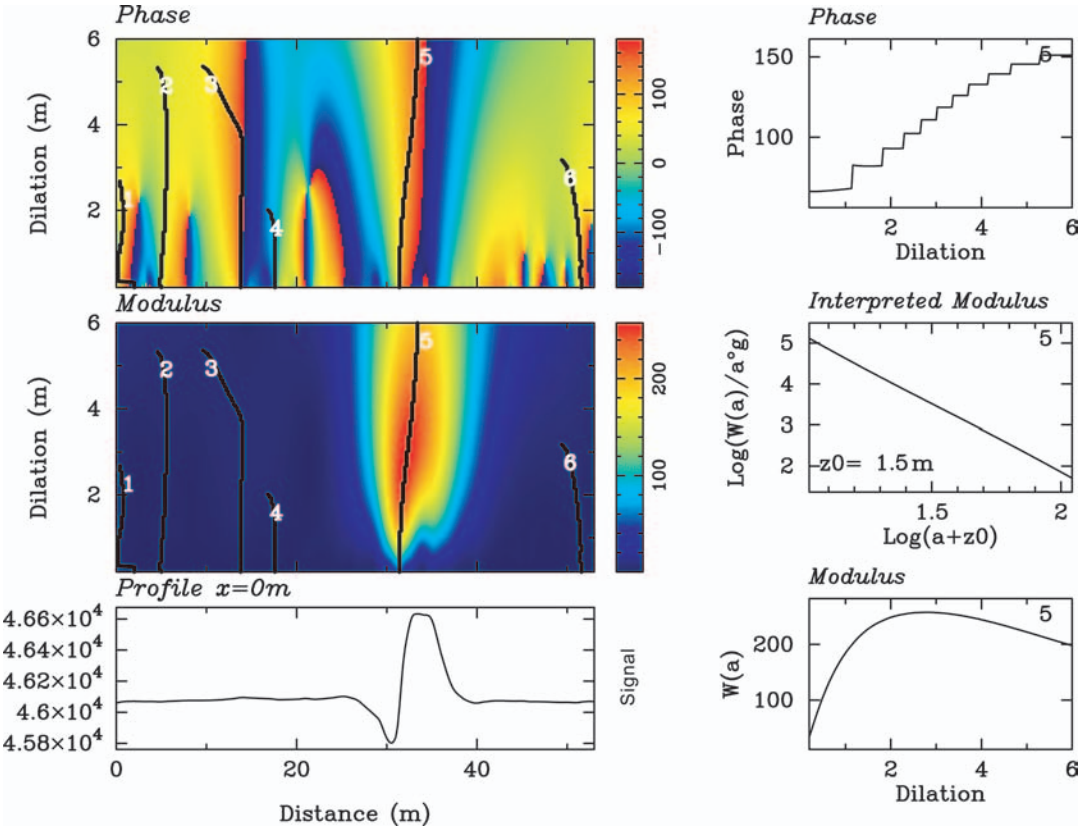

Figure 11. Complex multiscale tomography of anomaly T1, (profile $x = 0$ m). From top to bottom. Left: Phase; Modulus; Magnetic intensity. Right: Phase; Order α of the singularity ($\alpha \simeq -3.2$) and depth z (centre of the structure); Variation of the wavelet coefficient with respect to the dilation a (i.e. the depth z).

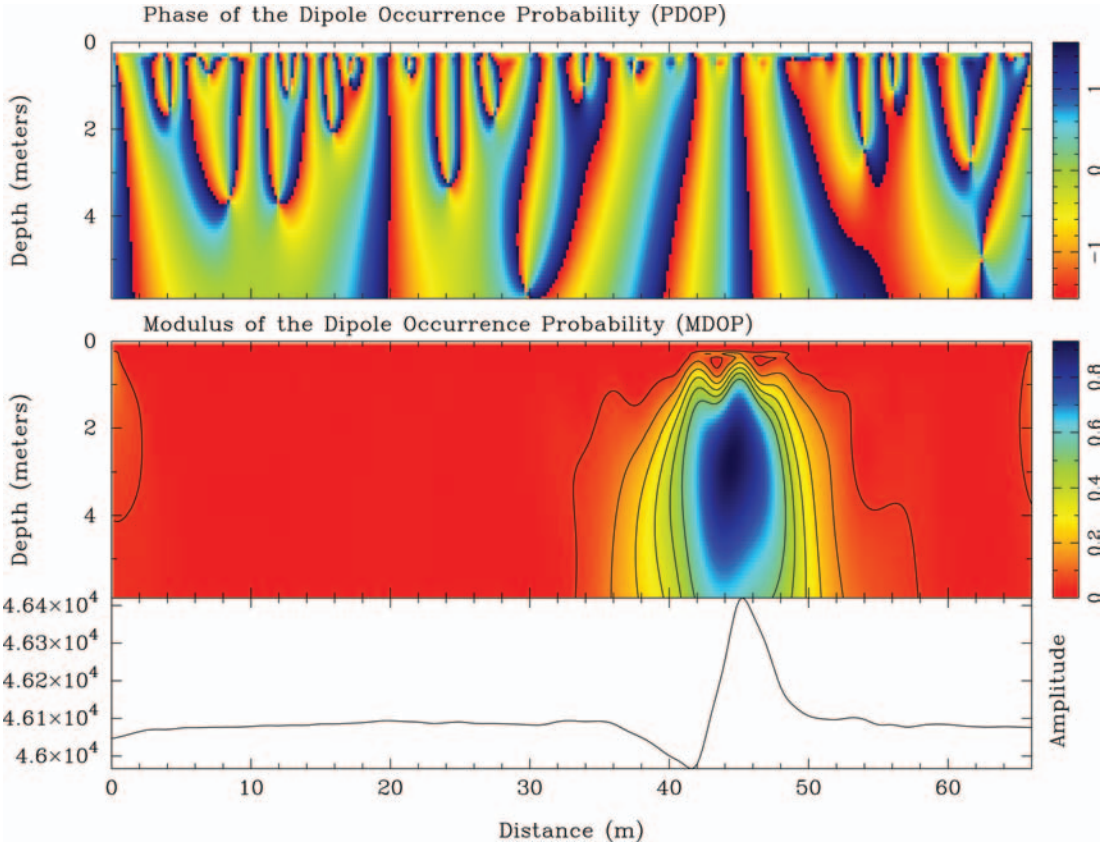

Figure 12. Complex dipolar occurrence tomography of anomaly T2, (profile $x = 2.5$ m, see Fig. 1). Top: Phase. Middle: Modulus. Bottom: Magnetic intensity.

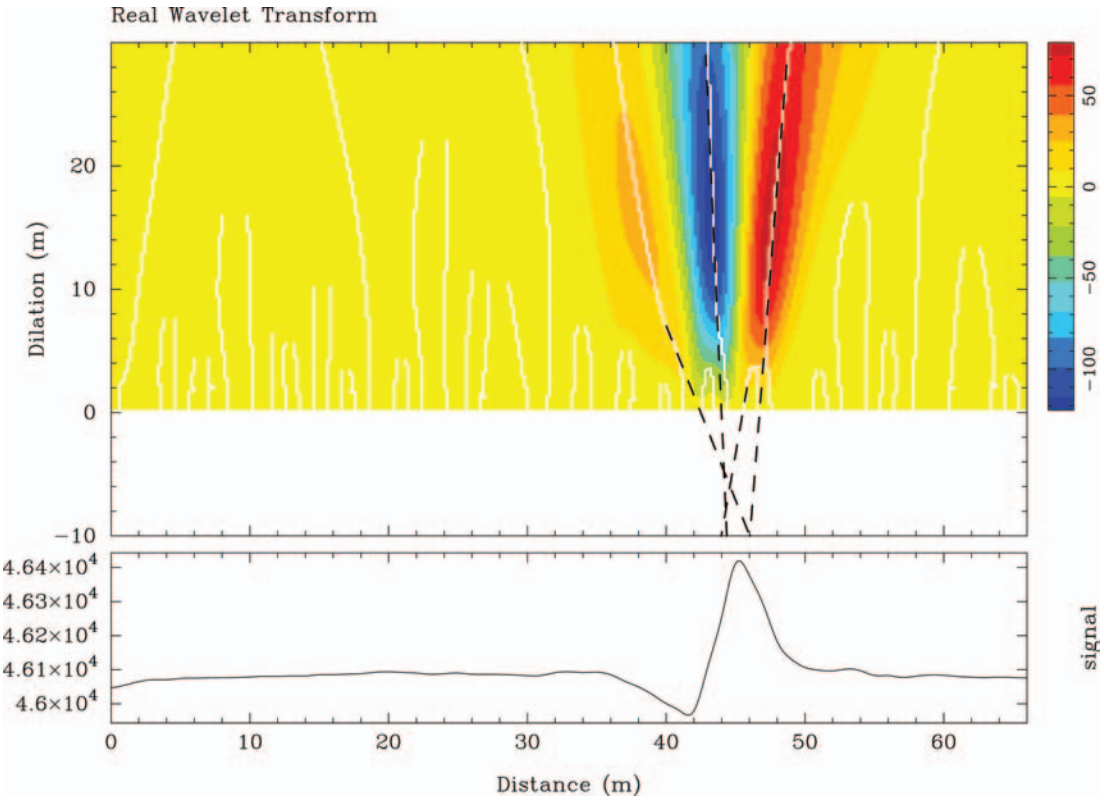

Figure 13. Real multiscale tomography of anomaly T2, (profile $x = 2.5$ m). The lines of extrema are presented by dashed lines. the dilation -10 represents a depth of 2 m, with a sample rate of 0.2.

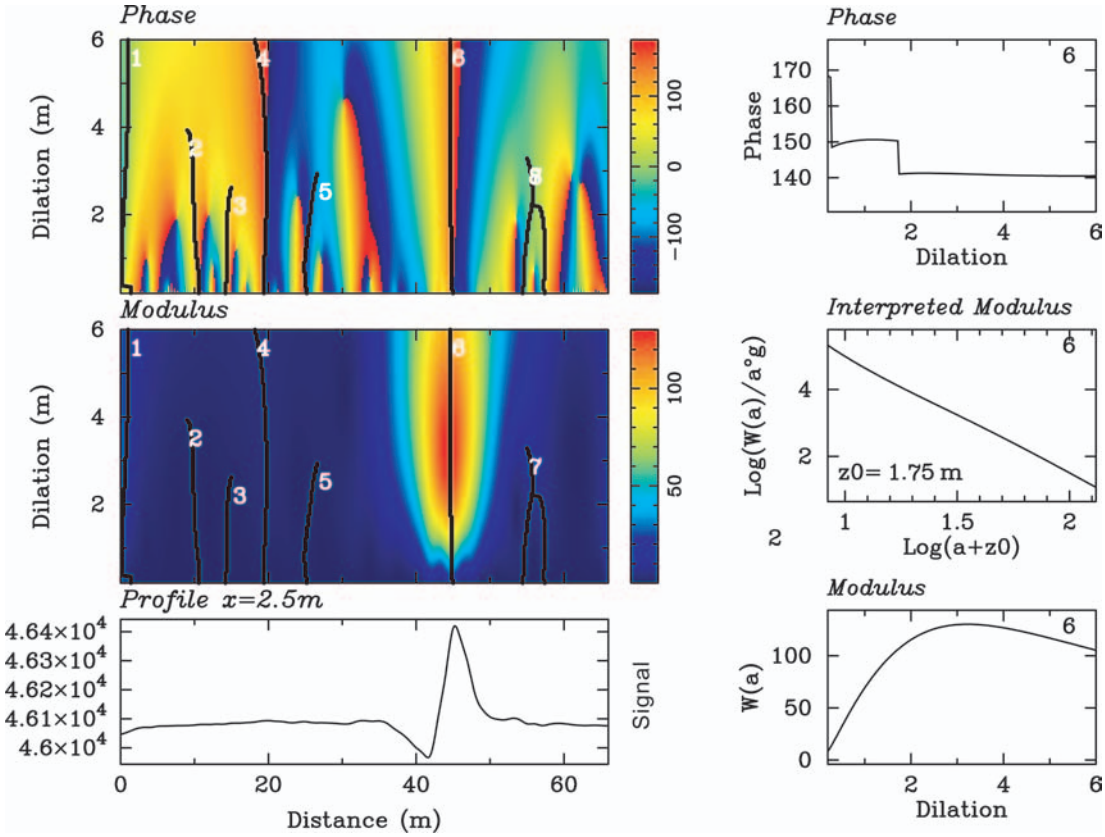

Figure 14. Complex multiscale tomography of anomaly T2, (profile $x = 2.5$ m). From top to bottom. Left: Phase; Modulus; Signal. Right: Phase; Order α of the singularity ($\alpha \simeq -3.7$) and depth z; Variation of the wavelet coefficient with respect to the dilation a (i.e. the depth z).

through the intersection point $z_s < 0$ gives the depth of magnetic buried sources (Fig. 2). This extension or extrapolation is similar to a contraction of the operator D in the half-plane $z < 0$. The degree α of buried sources or structures can be extracted from the slope β of extrema lines in log–log representation (Fig. 3) with respect to covariance and homogeneity properties of the CWT and the Poisson equation linking the source $\boldsymbol{\sigma}$ of dimension n and the potential anomaly A (Mallat & Hwang 1992; Moreau *et al.* 1997, 1999; Saracco *et al.* 2004). The detected effective source characterized by the local behaviour of the exponent α, we call this exponent the 'effective degree'. This 'effective degree' represents the homogeneous degree if the source is a homogeneous distribution. Let β be the degree of the magnetic field $\mathbf{B}$ which differs by one degree from the potential field, we have:

$$\mathbf{B} = -\boldsymbol{\nabla} A, \quad \Delta A(y,z) = -\boldsymbol{\sigma}(y,z) \Rightarrow \beta = \alpha + 1. \tag{7}$$

If we take an analysing wavelet not equal to the Poisson kernel P but to a partial derivative of P of order γ, using (1) and (6) the potential fulfils:

$$L_{(y,z)} A = \left(\frac{a}{a+z}\right)^{\gamma-2-\alpha} L_{[y(a+z)/a,1]} A \tag{8}$$

Accordingly,

$$\beta = 1 - \gamma + \alpha. \tag{9}$$

In one dimension a dipole (potential source) is a homogeneous function of degree $\alpha \simeq -2$, we consider here, sources of dimension 2 ($\alpha \simeq -3$) and we do not measure the potential but the field deriving from the magnetic potential.

3.3 Complex Poisson kernel

Introducing the Hilbert transform of the Poisson kernel P, we can define a complex Poisson kernel (Saracco *et al.* 2004). The complex Poisson kernel satisfies eq. (5), for complex potential fields. The complex analysing wavelet associated to the complex Poisson kernel, represents the analytic wavelet (in the sense of an 'analytic signal' (see Papoulis 1984) of the real wavelet g such that $g_a = \partial_y^\gamma \partial_z P + iHT[\partial_y^\gamma \partial_z P] = u^{\gamma-1} \exp^{-2\pi|u|} (i2\pi)^\gamma (u + i\,|u|)$. The choice of order γ of the partial derivative can be conditioned to increase energy through scales of the wavelet transform. We have chosen $\gamma = 2$; this implies an analysing wavelet with four vanishing moments. A phase and a modulus of the multiscale tomography of magnetic field can be defined (Fig. 4). If singularities are correctly extracted from the modulus, a good estimation of the depth of the object is obtained, while the phase allows us to define a new parameter: the inclination θ of structures for multipolar sources (Fig. 3, middle and Fig. 5, top) such that $\theta = -(90^\circ + Phase)$. For extended sources, we do not obtain a singular value θ, but a set of values where the modulus takes a maximal value. This set of values has a physical sense linked to the structure of the source along the analysed profile.

As a Roman oven is represented as a dipole magnetic source by palaeomagnetists, we have calculated the potential field generated by different dipole sources with different inclinations in presence of white Gaussian noise, then by multipole sources with the same inclination θ. The extrapolation of extrema lines out of the half-plane $z > 0$ is obtained from the calculus of straight lines from expression (9) using a least squares method. Fig. 2 presents the results of the real multiscale tomography of

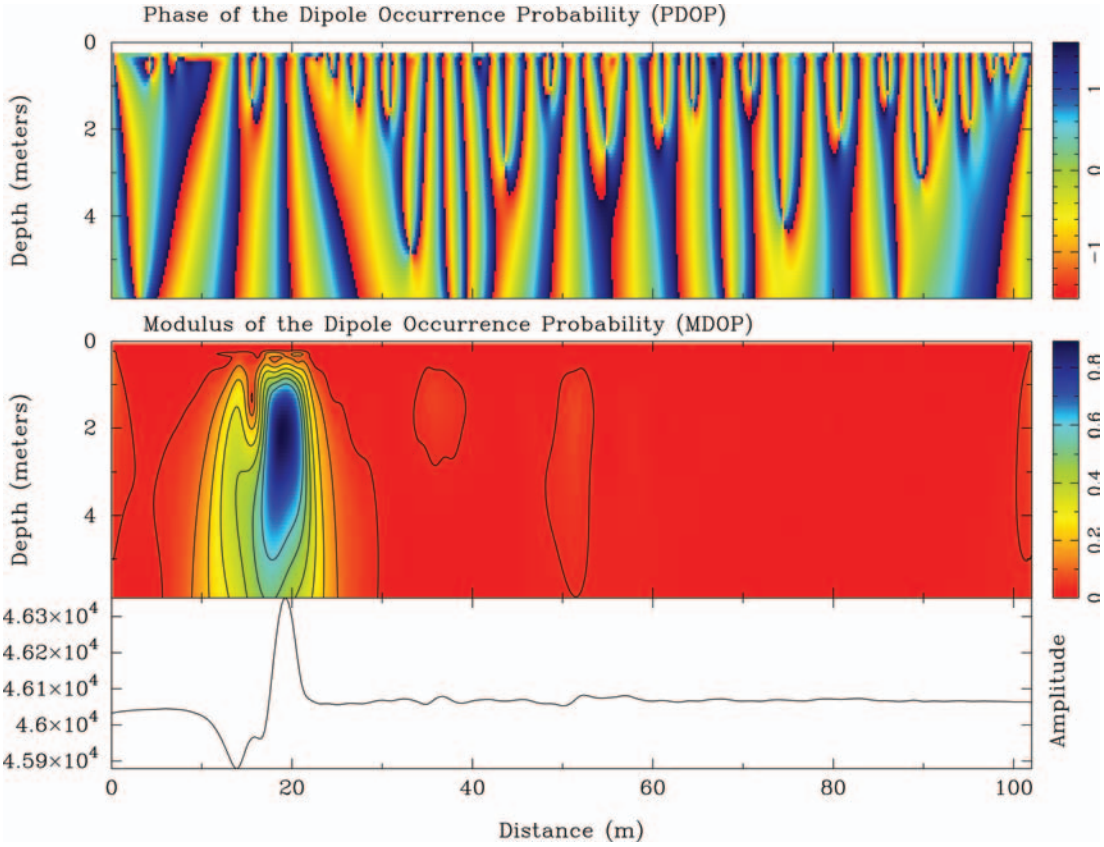

Figure 15. Complex dipolar occurrence tomography of anomaly T3, (profile $x = 27.5$ m, see Fig. 1). Top: Phase. Middle: Modulus. Bottom: Magnetic intensity.

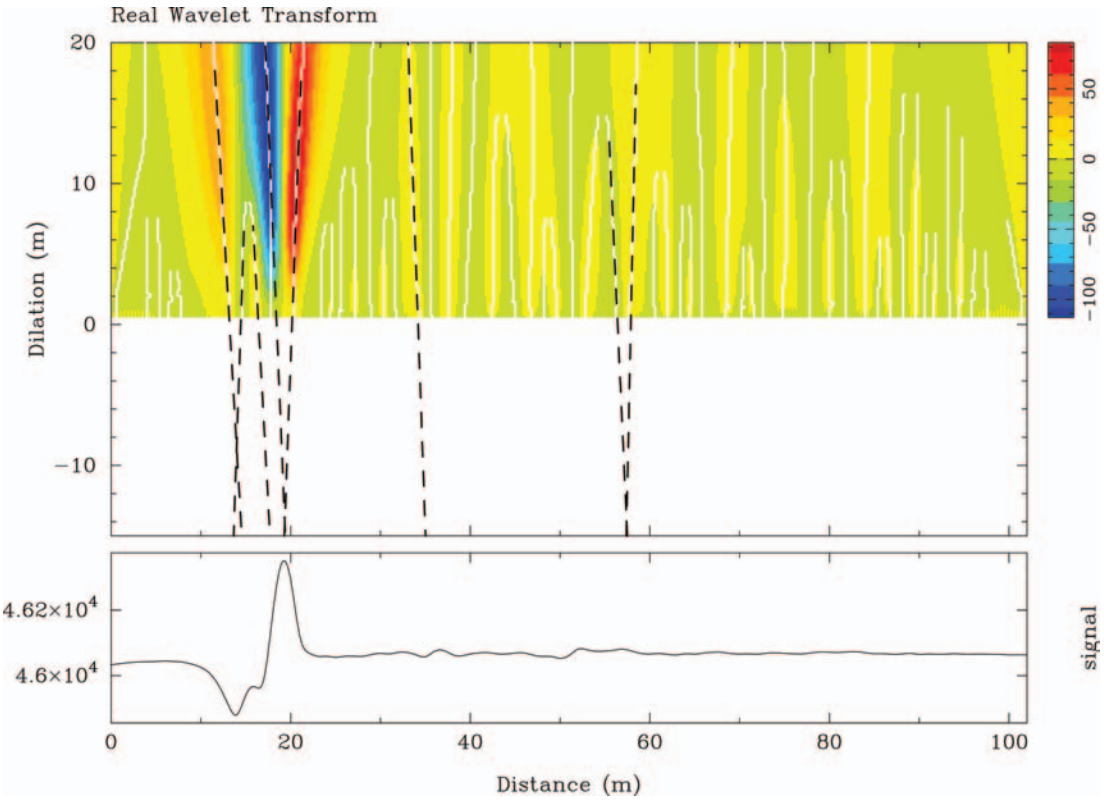

Figure 16. Real multiscale tomography of anomaly T3, profile $x = 27.5$ m. The lines of extrema are presented by dashed lines. The dilation −15 represents a depth of 3 m, with a sample rate of 0.2.

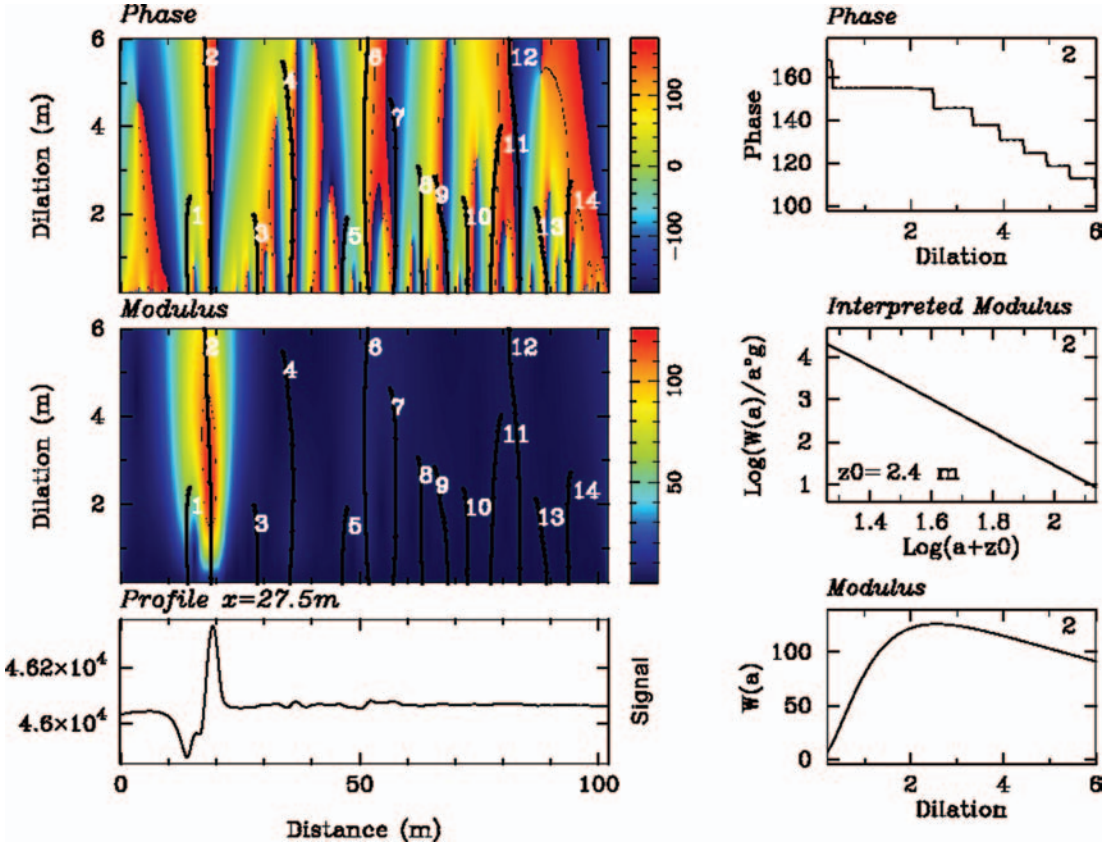

Figure 17. Complex multiscale tomography of anomaly T3, profile $x = 27.5$ m. Right: From top to bottom, phase, order α of the singularity ($\alpha \simeq -3.94$) and depth z, variation of the wavelet coefficient with respect to the dilation a (i.e. the depth z).

magnetic intensity in presence of noise generated by three dipole structures of different inclinations at lateral distances 500, 1000 and 1250 m and depth 50 m, while Fig. 3 presents results from complex wavelet tomography. The localization (Fig. 2) and the characterization of structures (Fig. 3) are, in spite of noise, in good accordance with the real values of depth, inclinations (30°, 90° and 0°) and homogeneity degree ($\beta = -4$). We note, from dilation 65, on the phase extracted from the CCWT (Fig. 3, middle), the influence of the third structure on the second one due to its closeness or coalescence. The amplitude variation along dilations (Fig. 3, bottom) is characteristic of a dipolar structure (see Fig. 5, bottom, for the dipole).

Figs 4 and 5 present the results of the complex wavelet tomography (or complex multiscale tomography) of the magnetic intensity in absence of noise generated by three multipolar structures (monopole of inclination 90°, dipole and quadrupole of inclination 0°) at lateral distances 750, 1500 and 2250 m, respectively, and depth 50 m. Results of inclinations and homogeneity degrees (Fig. 5, top and middle) are in good accordance with real values of θ and α (-2, -3.02 and -3.85). The depths of the structures obtained from real wavelet tomography are, respectively, 50.2, 50.5 and 48.1 m. Fig. 5, bottom, indicates the characteristic amplitude variations along dilations for multipoles.

4 COMPLEX DIPOLAR OCCURRENCE TOMOGRAPHY

This method, based on a normalized correlation between the measured potential anomalies $A(y, z > 0)$ and a supposed buried source, was introduced first by Patella in electrical tomography considering buried monopolar sources (Patella 1997). The localization of sources is obtained from the charge occurrence probability (COP). As dipolar sources are more appropriate for the search of magnetic archeological objects, one can define a dipolar charge occurrence probability (DOP) noted p, where $0 < p < 1$. The DOP represents vertical and horizontal components of the magnetic potential called the vertical and horizontal dipolar occurrence probability (Mauriello & Patella 1999). These two components can be interpreted as the real and imaginary parts of an analytic potential (Saracco *et al.* 2004). A modulus and a phase can be defined as the complex multiscale tomography. To avoid confusion between the dipolar occurrence probability tomography defined by Patella and this method defined in terms of modulus and phase, we call this one the complex dipolar occurrence tomography (CDOT). The modulus represents the dipolar charge occurrence and allows us to define the depth of buried sources supposed to be homogeneous of degree $\alpha \simeq -3$ in 2-D (dipolar potential sources). Inclinations of sources θ can be estimated from the phase of the complex dipolar tomography, as we have defined the inclination from the phase of the complex continuous wavelet transform. This means that the vertical lines of phase converging towards the detected sources, where the modulus is maximum, indicate the inclination θ of each source such that $\theta = -Phase$. The source signal Fig. 6 represents the 2-D magnetic intensity generated by a dipolar source in presence of noise at lateral distances 500, 1000 and 1250 m, respectively, ($\beta = -4$). The analysed signal is the same as Fig. 2. The inclination θ obtained for each source is, respectively, $\pi/6$, π and 0 (see Fig. 6, top) in perfect

Figure 18. Archaeological structures corresponding to anomalies T1 and T2 discovered after excavation.

Figure 19. Archaeological structures corresponding to the anomalie T3 discovered after excavation. We can observe archs corresponding to the top of the Roman oven.

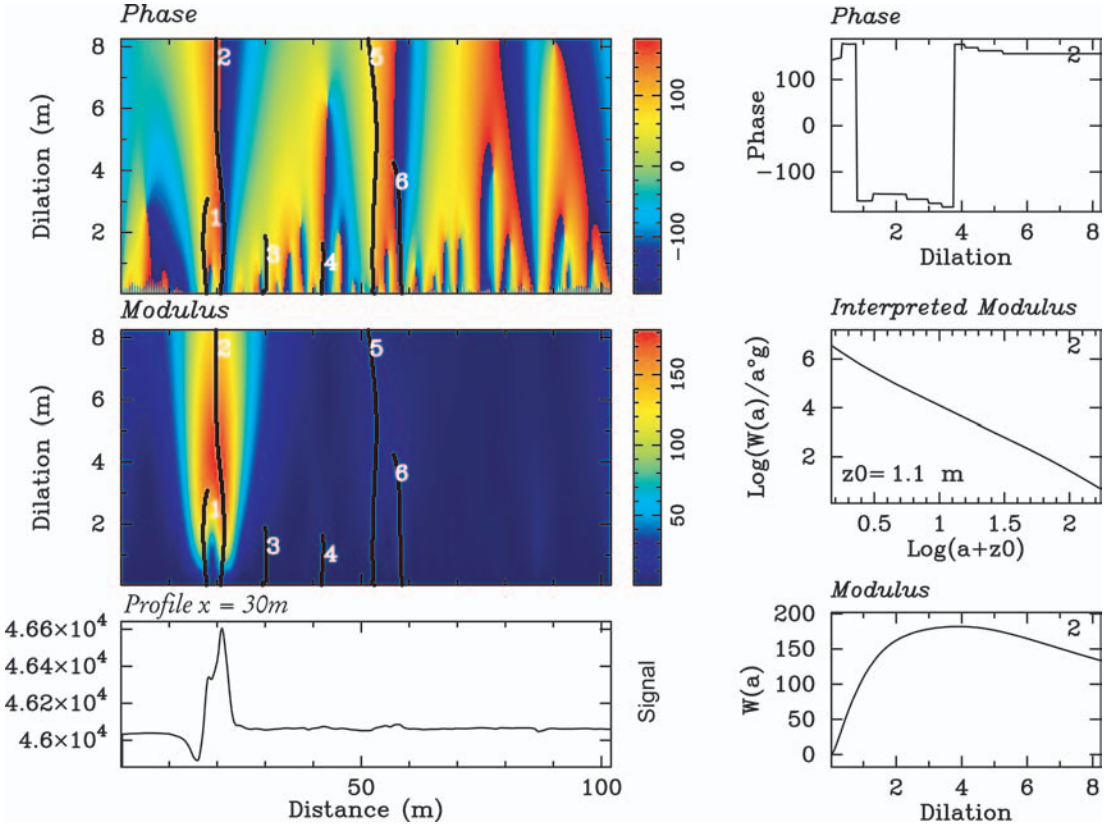

Figure 20. Anomaly T3: Multi-scale tomography for $x = 30$ m. Right: From top to bottom: Phase; Modulus; Measured magnetic intensity. Left: Phase; "effective degree" α with estimated depth z; and variation of the maxima of the modulus with respect to the dilation in the half-space $z > 0$.

accordance with true values, while their depths are obtained from the modulus of the CDOT with a dipolar occurrence probability value p of 0.25 (see Fig. 6, middle).

The use of dipolar tomography on magnetic intensity (Fig. 7) generated by a monopole, dipole and quadrupole structure without noise (same signal as Fig. 4) does not allow a correct localization and characterization of a multipole except when the source is dipolar (Fig. 7, middle). The modulus of the complex dipolar tomography cannot be equal to one even if the source is an isolated dipolar source in absence of noise (see Figs 6 and 7). This implies a rough estimation of the depth (see the impossibility to estimate the depth of sources). The advantage of using this method is to obtain a rapid estimation of possible buried isolated homogeneous structures and a good estimation of their inclinations. The values θ extracted from the phase of dipolar tomography are, respectively, π, 0 and 0 (Fig. 7, top).

5 ELECTRICAL RESISITIVITY AND EXPERIMENTS

To complete and compare our magnetic prospection of archeological structures, we made an electrical resistivity tomography of the site (Fig. 8). Three profiles of electrical resistivity were recorded at $x = 5$, 10 and 20 m with a LUND SAS-4000 acquisition system (see Fig. 1). We choose a Wenner protocole for a good signal-to-noise ratio, including 64 electrodes of 1 m spacing. Tomographic sections were obtained with the academic RES2DINV software of LUND. Potential archeological structures appear along profiles 13, 14, 15 in agreement with some magnetic anomalies (Fig. 8). High values of resistivity appear also for a strong compaction of the ground. In this case, it is difficult to distinguish the contribution due to the lithological structure of the ground from the contribution of archeological structures, without palaeomagnetic information.

Potential archeological structures (Fig. 8) (antique ovens) appear as local resistive objects of (40–120 Ω m) range, at the depth of 1–2 m, buried in sediments (10–30 Ω m). The limestone substrate appears at large depth with a resistivity of (60–230 Ω m). The problem of this method is to differentiate, sometimes, an archeological object from natural subsurface heterogeneities such as local compaction of the ground, change of soil mineralogy, or from the limestone substrate. They could give the same electrical resistivity or conductivity behaviour. Only the information carried by the remanent magnetic field allows us to separate an archeological structure from the surrounding rock. Conjoint electrical and magnetic surveys are necessary.

6 MULTISCALE AND COMPLEX DIPOLAR OCCURRENCE TOMOGRAPHY: RESULTS ON FIELD DATA

We found different depths and inclinations of structures corresponding to archeological objects (fragment of tiles, broken potteries, etc.), and lithological objects (clays, limestone substrate) (see Figs 1 and 8). Each structure is spatially localized and characterized by its amplitude, degree and phase. We present results both in real (Figs 10, 13 and 16) and complex multiscale tomography (Figs 11, 14, 17, 20 and 21), and in complex dipolar occurrence tomography (Figs 9, 12 and 15). Inclinations versus dilation are obtained from the phase φ

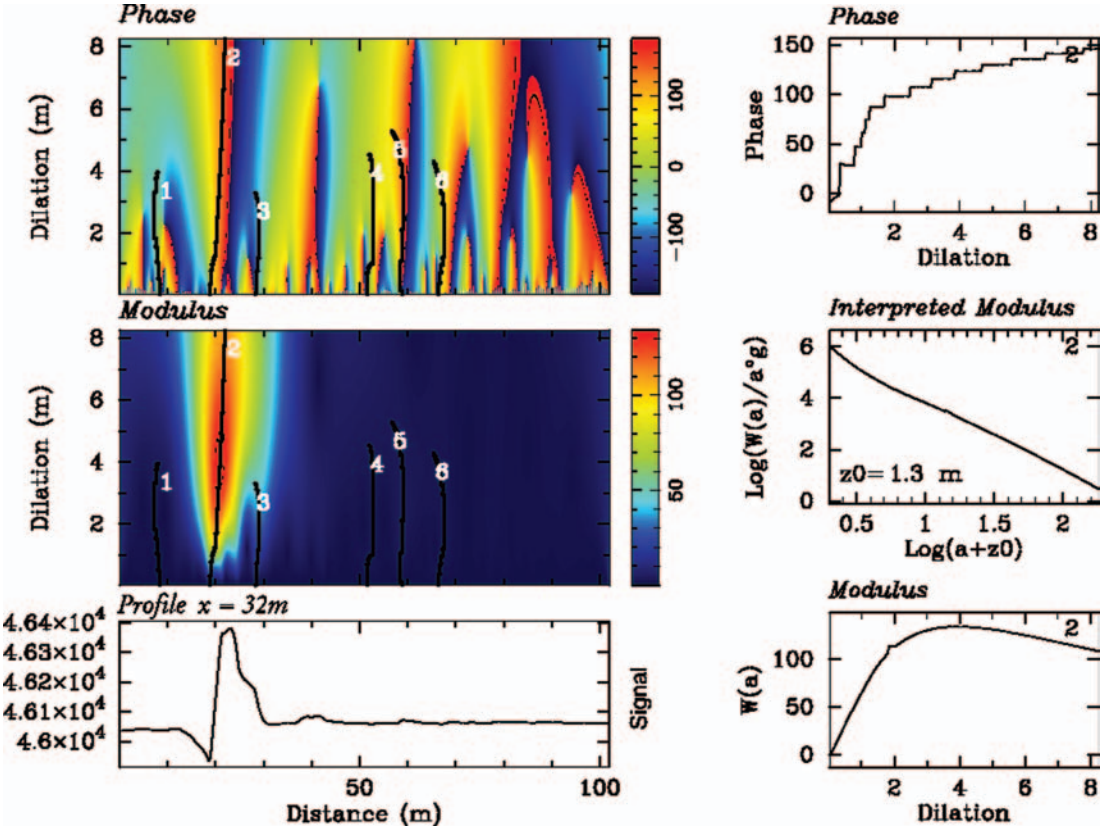

Figure 21. Anomaly T3: Multi-scale tomography for $x = 32$ m. Right: From top to bottom: Phase; Modulus; Measured magnetic intensity. Left: Phase; "effective degree" α with estimated depth z; and variation of the maxima of the modulus with respect to the dilation in the half-space $z > 0$.

of the CMST, such that $\theta = -(90^o + \varphi)$. The degree of elementary structures is obtained from the slope of extrapolated lines of extrema in the half-plane $z < 0$ versus $\log |L_{(y,z)}/a^\gamma)|$, $|\mathrm{Log}(a + z0)|$.

We notice three main anomalies denoted T1, T2, T3, of which the last, T3, is very extented. To obtain a better estimation of depths, magnetic data were interpolated with a sample rate of 0.2 m. The ordinates of the real multiscale tomography are displayed until the dilation value -10 (Figs 10 and 13) and -15 (Fig. 16). The depths associated to these scale values are, respectively, -2 and -3 m. Real and complex multiscale tomography are displayed on 6 octaves of 50 voices each, from the first dilation $a = 0.5$.

The lines of extrema and ridges of the multiscale tomography are numbered (Figs 11, 14 and 17). Only ridges corresponding to main anomalies are presented, that is, ridges 5, 6 and 2 for anomalies T1, T2 and T3, respectively. From the phase of the CMST, we determine a set of inclinations θ linked to the structure of buried sources while the intersection of the lines of extrema of the RMST, gives an estimate of the depth z and the 'effective degree' α of source.

From the phase of the complex dipolar occurrence tomography we extract, when the modulus is maximum, the inclination of structures (Top of Figs 9, 12 and 15). The estimated depth corresponds to the high magnetization part of ovens. To characterize the depth and the 'effective degree' from wavelet tomography, we have the choice to analyse the structure in its globality, and to extract a mean depth of the structure from the complex wavelet tomography, or to consider a local analysis and extract from the real wavelet tomography a local variation of the remanent magnetization of the structure.

The results for the multiscale tomography (real and complex) and complex dipolar occurrence tomography (CDOT) are summarized in Tables 1 and 2. A 0.8 m correction for the probe height was made. The depths deduced from multiscale tomography (MST) are, respectively (0.49 and 0.69 m) for T1 anomaly and (0.9 and 1.2 m) for T2 anomaly.

Results of the larger and deeper T3 anomaly are summarized in Table 2. Figs 20 and 21 complete the results for profiles $x = 30$ and 32 m.

7 RESULTS OF ARCHAEOLOGICAL EXCAVATION

Excavations were made on the Fox-Amphoux site by archeologists. They found Roman ovens on magnetic anomalies locations. The dimensions of kilns were: 2 m wide by 2–3 m high. The depths found were in agreement with results obtained from wavelet tomography (Figs 18 and 19). Only the top of anomaly T3 was excavated (Fig. 19). The strong and wide anomaly observed in this place using both electrical and magnetic surveys is due to the presence of a depot of blows. The Roman oven (anomaly T1) was partially broken down (Fig. 17), and was discovered after the first 0.7 m of clearing, corresponding to the estimated depth values. Each structure possesses its own magnetic field, because the overheated earth has a different magnetization from the natural magnetic environment rock. Potteries (overheated earth) contain magnetic minerals, principally iron oxides, responsible for remanent magnetization. When the temperature reaches the Curie or Neel temperature, during the firing, this remanent magnetization disappears. During the cooling below this critical temperature, a new remanent magnetization is acquired, guided by the surrounding magnetic field. This new remanent

Table 1. Results for T1 and T2 magnetic anomalies.

Lateral position x (m)	y (m)	MST depth z (m)	CDOT Probability p for z (m)
0	31.53	0.49	$p = 1$ for $0.5 < z < 1.5$
0	35.24	0.69	$p = 0.7$ for $1.2 < z < 2$
2.5	45.9	0.90	$p = 1$ for $0.4 < z < 1.3$
2.5	46.8	1.2	$p = 1$ for $0.4 < z < 1.3$

Table 2. Results for T3 manetic anomaly.

Lateral position x (m)	y (m)	MST depth z (m)	CDOT Probability p for z (m)
22.5	12.51	0.86	$p = 0.4$ for $1.8 < z < 3.8$
22.5	53	1.63	$p = 0.15$ for $0.3 < z < 1.7$
25	11.65	0.66	$p = 0.2$
25	18.18	1.49	$p = 0.7$ for $0.3 < z < 1.7$
27.5	13	0.86	$p = 0.3$
27.5	19.28	1.82	$p = 0.9$ for $1.1 < z < 2.1$
27.5	35.2	2.32	$p = 0$
27.5	57	2	$p = 0$
30	17	1.4	$p = 0.6$ for $2 < z < 3$
30	21.29	1.25	$p = 0.8$
30	22.82	0.84	$p = 0.4$
30	57	3.81	$p = 0$
32	19.57	0.53	$p = 0.4$
32	26.3	6.3	$p = 0$
32	41.57	0.94	$p = 0$

magnetization is then a record of the field during the cooling. Complementary analysis of rock magnetic and on archaeological fragments sampled during our experiments have shown a dominant natural remanent magnetization (NRM). We have studied only results corresponding to potential ovens and archaeological fragments with strong magnetizations. To complete T3 anomaly analysis, we present complex wavelet tomography for $x = 30$ and 32 m (Figs 20 and 21) showing estimated depth structures around 1.3–1.5 m. This is in agreement with the depth obtained by archeologists after excavation.

8 CONCLUSION AND PERSPECTIVES

The total magnetic field anomalies found by caesium magnetometer surveys may arise from the superimposition of induced and NRM of archeological structures. Classical magnetic instruments sometimes restrict the search of burial objects from potential anomalies due to induced magnetizations only. It appears from the rock magnetic study of Fox-Amphoux site, that NRM dominates, if it is not weakened by induced chainage anisotropy. In this case classical methods are not well adapted. The multiscale tomography applied to the total magnetic field makes it possible to estimate the depth of potential sources in terms of modulus and phase, whatever their origin, either induced or remanent. A complex structure is decomposed into 'effective' sources, or isolated singularities for which estimates are obtained for inclinations, depth and 'effective' degree. The depths estimated by our methods are in good agreement with the size and the structure of archaeological objects excavated by archeologists on cultivated field at Fox-Amphoux site (Var). Moreover we obtained information on the localization of lithological structure (limestone substratum), and on archeological fragment objects of the same century (fragments of kiln, tiles, potteries, etc.).

The estimates of inclinations of structures from the phase of complex dipolar tomography or multiscale tomography for synthetic noisy isolated homogeneous sources, are satisfactory. For extended sources like Roman ovens, it seems that the phase taken along the maxima of the modulus makes a physical sense. The results obtained for the anomalies T2 and T3 are in good agreement with structures excavated. The results for the anomaly T1 are not clear because of the small depth of the excavated oven, destroyed in major part by agricultural activity over time.

This study demonstrates the efficiency of multiscale tomography methods in archaeological prospecting and we want to develop this processing to deeper complex archaeological structures.

ACKNOWLEDGMENTS

We want to thank F. Laurier, archeologist of DRAC-Toulon, M. Delestre, archeologist of DRAC-Marseille, Region PACA, for their advice and financial support, J. J. Motte for his help on some graphics, P. Rochette for his advice on palaeomagnetism and A. Grossmann for fruitful discussions on continuous wavelet transforms and theory of distributions. We want to thank the referees and the editor for their constructive remarks.

REFERENCES

Alexandrescu, M., Gibert, D., Hulot, G., Lemouel, J.L. & Saracco, G., 1995. Detection of geomagnetic jerks using wavelet analysis, *J. geophys. Res.,* **101**(B10), 21 975–21 994.

Blakely, R.-J., 1995. *Potential Theory in Gravity and Magnetic Applications*, Cambridge University Press, New York.

Brizzolari, E., Ermolli, F., Orlando, L., Piro, S. & Versino, L., 1994. Integrated geophysical methods in archaeological surveys, *J. appl. Geophys.,* **29,** 47–55.

Courant, R. & Hilbert, D., 1962. *Methods of Mathematical Physics,* Vol. 2, Intersciences Publisher, J. Wiley and Sons, New York.

Corwin, R.F., 1990. The self-potential method for environmental and engineering applications, Geotechnical and Environmental Geophysics, Vol. 1, *Review and Tutorial*, pp. 127–146, ed. Ward, S.H., Society of Exploration Geophysicists, Tulsa, OK, USA.

Durrheim, R.J. & Cooper, G.R.-J., 1998. EULDEP: a program for the Euler deconvolution of magnetic and gravity data, *Comput. Geosci.,* **24,** 545–550.

Delprat, N., Escudie, B., Guillemain, P., Kronland-Martinet, R., Tchamitchian, P. & Torresani, B., 1991, Tech. rep. CPT-91, no P. 2512, Luminy, Marseille, France.

Grossmann, A., 1986. Wavelet transforms and edge detection, in *Stochastic Process in Physics & Eng.*, pp. 149–157, eds Blanchard, P., Streit, L. & Hazewinkel, M., Reidel Pub. Co., New York.

Grossmann, A. & Morlet, J., 1984. Decomposition of Hardy functions into square integrable wavelets of constant shape, *Soc. Int. Am. Math. J. Anal.,* **15,** 723–736.

Grossmann, A., Holschneider, M., Kronland-Martinet, R. & Morlet, J., 1987. Detection of abrupt changes in sound signals with the help of wavelet transforms, in *Inverse Problem: An Interdisciplinary Study,* Vol. 19, Adv. Elect. Phys. Supp., pp. 289–306, Academic Press, San Diego.

Guillemain, P., 1994. Estimation de lignes spectrales par transformée en ondelettes: application aux signaux de spectroscopie RMN, *Thèse*, Univ. Aix-Marseille II, Marseille, France.

Hornby, P., Boschetti, F. & Horowitz, F.G., 1999. Analysis of potential field data in the wavelet domain, *Geophys. J. Int.,* **137,** 175–196.

Ishido, T. & Pritchett, J.W., 1999. Numerical simulation of electrokinetic potential associated with subsurface flow, *J. geophys. Res.,* **104,** 15 247–15 259.

Jeng, Y., Lee, Y.L., Chen, C.-Y. & Lin, M-J, 2003. Integrated signal enhancements in magnetic investigation in archeology, *J. appl. Geophys.,* **53,** 31–48.

Lapenna, V., Patella, D. & Piscitelli, S., 2000. Tomographic analysis of self-potential data in a seismic area of Southern Italy, *Annali di Geofisica,* **43,** 361–373.

Mallat, S. & Hwang, W.L., 1992. Singularity detection and processing with wavelets, *IEEE Trans. Inf. Theory.,* **38,** 617–643.

Martelet, G., Sailhac, P., Moreau, F. & Diament, M., 2001. Characterization of geological boundaries using 1D wavelet transform on gravity data, theory and application to the Himalayas, *Geophysics,* **66,** 1116–1129.

Marson, I. & Klingele, E.E., 1993. Advantages of using the vertical gradient of gravity for 3-D interpretation, *Geophysics,* **58**(11), 1588–95.

Mauriello, P. & Patella, D., 1999. Principles of probability tomography for natural-source electromagnetic induction fields, *Geophysics,* **64**(5), 1403–1417.

Mauriello, P., Monna, D. & Patella, D., 1998. 3D geoelectic tomography and archeological applications, *Geophys. Prospect.,* **46,** 543–570.

Moreau, F., 1995. Méthodes de traitement de données géophysiques par transformée en ondelettes, *Thèse, Campus de Beaulieu,* Rennes, France.

Moreau, F., Gibert, D., Holschneider, M. & Saracco, G., 1997. Wavelet analysis of potential fields, *Inv. Probl.,* **13,** 165–178.

Moreau, F., Gibert, D., Holschneider, M. & Saracco, G., 1999. Identification of sources of potential fields with the continuous wavelet transform: basic theory, *J. geophys. Res.,* **104,** 5003–5013.

Nabighian, M.N., 1984. Toward a three-dimensional automatic interpretation of potential field data via generalized Hilbert transforms: Fundamental relations, *Geophysics,* **49**(6), 780–786.

Noel, M. & Xu, B., 1991. Archaeological investigation by electrical resistivity tomography: A preliminary study, *Geophys. J. int.,* **107,** 95–62.

Papoulis, A., 1984. *Probability, Random Variables and Stochastic Processes*, McGraw-Hill, Inc, New York.

Parker, R.L., 1994. *Geophysical Inverse Theory*, Princeton Univ. Press, New Jersey.

Parker, R.L. & Huestis, S.P., 1974. The inversion of magnetic anomalies in the presence of topographic effect, *J. geophys. Res.,* **79,** 1587–1593.

Patella, D., 1997. Introduction to ground surface self potential tomography, *Geophys. Prospect.,* **45,** 653–681.

Ravat, D., 1996. Analysis of Euler method and applicability in environmental magnetic investigations, *J. Elect. E G,* **1**(3), 229–238.

Reid, A.B., Allsop, J.M., Granser, H., Millett, A.J. & Somertom, I.W., 1990. Magnetic interpretation in three dimensions using Euler deconvolution, *Geophysics,* **55**(1), 80–91.

Sabatier, P.C. (Ed.), 1987. *Inverse Problem: An Interdisciplinary Study*, Academic Press, London.

Sailhac, P. & Marquis, G., 2001. Analytic potentials for the forward and inverse modeling of SP anomalies caused by subsurface fluid flow, *Geophys. Res. Lett.,* **28,** 1851–1854.

Saracco, G., 1989. Acoustic propagation of harmonic and transient signals through an inhomogeneous medium: asymptotic methods and Wavelet transforms, *Thèse de Doctorat*, University of Luminy, Marseille, France.

Saracco, G., Gazanhes, C., Sageloli, J. & Sessarego, J.P., 1990a. Time-scale analysis of acoustic scattering by elastic spherical shells for impulse sources, *J. Acoust.,* vol. **3**(4), 381–392.

Saracco, G., Guillemain, P. & Kronland-Martinet, R., 1990b. Characterization of elastic shells by the use of wavelet transform, *IEEE- Ultrasonic Symp.,* **2,** 881–885.

Saracco, G., Labazuy, P. & Moreau, F., 2004. Localisation of self-potential sources in volcano-electric effect with complex continuous wavelet transform and electrical tomography methods for an active volcano, *Geophys. Res. Lett.,* **31** L12610, doi:10.1029/2004GL01954.

Saracco, G., Sessarego, J.P., Sageloli, J., Guillemain, P. & Kronland-Martinet, K., 1991. Extraction of modulation laws of elastic shells by the use of the wavelet transform, pp. 61–68, *Research notes in Applied Mathematics, series* eds Ciarlet, P.J. & Lions, J.L., Wavelets and Applications, ed. Meyer, Y., Masson-Springer-Verlag, Paris.

Tarantola, A., 1987. *Inverse Problems Theory: Methods for Data Fitting and Model Parameter Estimation*, Elsevier, New York.

Telford, W.M., Geldart, L.P., Sheriff, R.E. & Keys D.A., 1990. *Applied Geophysics*, 2nd ed., 770 p., Cambridge University Press, New York.

Thompson, D.T., 1982. Euldph: a new technique for making computer assisted depth estimates from magnetic data, *Geophysics,* **47**(1), 31–37.

Tsokas, G.N. & Papazachos, C.B., 1992. Two dimensional inversion filters in magnetic prospecting: application to the exploration for buried antiquities, *Geophysics,* **57,** 1004–1113.

Zhdanov, M.S. & Keller, G.V., 1994. *The Geoelectrical Methods in Geophysical Exploration*, Elsevier, New York.